

# Chapter 4

## Squeeze film characteristics between a sphere and a flat porous plate

### Contents

---

- 4.1 Introduction
  - 4.2 Development of the Mathematical Model
  - 4.3 Solution
  - 4.4 Results and Discussion
    - 4.4.1 Discussion on Squeeze Film Pressure
    - 4.4.2 Discussion on Load Carrying Capacity
    - 4.4.3 Discussion on Squeeze Film Time
    - 4.4.4 Representative Values and Calculation of  $K$
  - 4.5 Conclusions
  - 4.6 Figures
  - 4.7 References
-

## 4.1 Introduction

When two lubricated surfaces approach each other with a normal velocity (known as squeeze velocity), then squeeze film phenomenon arise [1]. Study of squeeze film behaviour are observed in many fields of real life such as in machine tools, gears, rolling elements, hydraulic systems, engines, clutch plates, etc. Also, it is observed in the study of human knee joints and other skeletal joints as bio-lubrication [2]. Squeeze film with the attachment of porous layer (region or plate or matrix or surface) are widely used in industry because of its advantageous property of self-lubrication and no need of exterior lubricant supply.

In recent years, many theoretical and experimental inventions are made on the bearing design systems as well as on the lubricating substances in order to increase the efficiency of the bearing performances. One of the major revolutions in the direction of lubricating substances is an invention of ferrofluids (FFs). Many researchers have also tried to find its application as lubricant in squeeze film bearing design systems. Verma [3] studied effects of magnetic fluid (MF) on squeeze film bearing design system under an externally applied magnetic field oblique to the lower surface with the lower porous surface composed of three thin layers with different porosities. Explicit solutions for velocity, pressure, load carrying capacity and response time are obtained. It is found that upper plate takes longer time to come down in this case as compared to conventional lubricant based squeeze film. Kumar *et. al.* [4] studied squeeze film for spherical and conical bearings using ferrofluid (FF) as lubricant with the effects of rotation of particles and constant magnetic field in transverse direction, and numerically studied various bearing characteristics. Bhat and Deheri [5] discussed about curved porous circular discs squeeze film with the effect of MF and shown that pressure, load carrying capacity and response time increases with the increase of magnetization. Prajapati [6] discussed various designed squeeze

films with MF effect and shown the superiority performance of the MF lubricant than conventional lubricant. Shah *et. al.* [7] studied squeeze film between porous annular curved plates with the effects of rotational inertia as well as MF and found that the increase in pressure and load carrying capacity depended only on the magnetization whereas response time dependent on magnetization, fluid inertia and speed of rotation of the plates. In [8], Shah and Bhat studied squeeze film in a long journal bearing using FF as lubricant and found that load carrying capacity and response time increased with the increasing values of the eccentricity ratio. In [9], Patel and Deheri discussed about MF based squeeze film between porous conical plates and found that negative effect induced by the porosity can be neutralized by the positive effect caused by the magnetization parameter. Andharia and Deheri in [10] studied MF based squeeze film for truncated conical plates with the effect of longitudinal roughness and found that load carrying capacity can be increased with magnetization as well as negatively skewed roughness. The pressure and response time also found to increase with magnetization. Shah and Patel [11] discussed impact of various porous structures on curved porous circular plates squeeze film using FF as lubricant and found that globular sphere model have more impact on increase of load carrying capacity as compare to capillary fissures model. Lin *et. al.* in [12] studied squeeze film characteristics for conical plates with the effect of fluid inertia and FF, and shown the better performance of the system as compared to non-inertia non-magnetic case. In [13], Lin *et. al.* studied squeeze film characteristics of parallel circular discs with the effects of FF and non-Newtonian couple-stresses using transverse magnetic field. With these effects, it was shown that higher load carrying capacity and lengthens approaching time obtained.

The purpose of the present Chapter is to study newly designed squeeze film bearing made up of a sphere and a flat plate using water based FF as lubricant, which is controlled by

oblique and variable magnetic field, with the effects of porosity, slip velocity and squeeze velocity. With these effects, the impact of squeeze film height, permeability and width of the porous layer are studied. Expressions for pressure, load carrying capacity and response time are obtained from Reynolds equation. The dimensionless pressure distribution, load carrying capacity and response time are calculated and presented graphically.

## 4.2 Development of the Mathematical Model

Figure 4.1 shows the schematic representation of the bearing design system under study. The upper surface is a rigid sphere of radius  $a$ , and lower surface is a flat porous plate which is formed when a porous layer of thickness  $H_0$  is attached to the impermeable flat surface. The porous layer is considered because of added advantage of self-lubricating property of the system. The region between the sphere and flat porous plate is known as film region, which is filled with FF and controlled by variable magnetic field of strength  $H$ , which is oblique to the lower plate. As far as dynamical part is concern, the upper surface (sphere) approaches to lower flat porous plate with a uniform velocity, known as squeeze velocity  $\dot{h}_m$ , and is defined as

$$\dot{h}_m = \frac{dh_m}{dt}, \quad \dots (4.1)$$

where  $h_m$  is minimum film thickness and  $t$  is time.

The shape of the film thickness  $h$  is defined as

$$h = h_m + \frac{r^2}{2a}; \quad r \ll a,$$

... (4.2)

where  $r$  is the radial coordinate.

Also,

$$\mathbf{q} = (\dot{r}, r\dot{\theta}, \dot{z}) = (u, rv, w),$$

... (4.3)

where  $(r, \theta, z)$  are cylindrical coordinates and dot ( $\dot{\phantom{x}}$ ) represents derivative with respect to  $t$ .

As mentioned above, the variable magnetic field of strength  $H$  considered here is of the form [14]

$$H^2 = \frac{K r^2 (a - r)}{a},$$

... (4.4)

where  $K$  is chosen to suit the dimensions of both sides.

By combining equations (2.18) to (2.22) and using equation (4.3) under usual assumptions of lubrication, neglecting inertia terms, and that the derivatives of fluid velocities across the film predominate, the equation governing the lubricant flow in the film region in cylindrical coordinates yields

$$\frac{\partial^2 u}{\partial z^2} = \frac{1}{\eta} \frac{d}{dr} \left( p - \frac{1}{2} \rho_0 \bar{H}^2 \right),$$

... (4.5)

where  $p$  is the pressure in the film region,  $\sim_0$  is the free space permeability,  $\bar{\sim}$  is the magnetic susceptibility and  $y$  is the fluid viscosity.

As porous layer is attached to the lower impermeable surface, solving equation (4.5) using slip boundary condition at the lower porous surface (that is, at  $z = 0$ ) as (refer [15, 16])

$$u = \frac{1}{s} \frac{\partial u}{\partial z}; \frac{1}{s} = \frac{\sqrt{w_r y_r}}{5},$$

and condition at the upper spherical surface as

$$u = 0 \text{ when } z = h,$$

yields velocity profile in the film region as

$$u = \frac{\{h + z(1 + sh)\} (z - h)}{2y(1 + sh)} \frac{d}{dr} \left( p - \frac{1}{2} \sim_0 \bar{\sim} H^2 \right),$$

... (4.6)

where  $s$  is a slip parameter and  $w_r, y_r$  are the permeability and porosity of the porous region in the radial direction respectively.

The continuity equation for the film region in cylindrical coordinates is given by

$$\frac{1}{r} \frac{\partial}{\partial r} (ru) + \frac{\partial w}{\partial z} = 0,$$

... (4.7)

which on integrating over the film thickness  $h$ ; that is, over the interval  $(0, h)$  and making use of equation (4.6) with the insertion of squeeze velocity effect  $w_h = w|_{z=h} = \dot{h}_m$ , yields

$$\frac{1}{r} \frac{\partial}{\partial r} \left[ \frac{rh^3(4+sh)}{12\gamma(1+sh)} \frac{d}{dr} \left( P - \frac{1}{2} \sim_0 \bar{H}^2 \right) \right] = \dot{h}_m - w_0, \text{ where } w_0 = w|_{z=0}.$$

... (4.8)

Assuming the validity of the Darcy's law in the porous region, the radial and axial velocity components of the fluid in the porous region are given by

$$\bar{u} = -\frac{w_r}{\gamma} \left[ \frac{\partial}{\partial r} \left( P - \frac{1}{2} \sim_0 \bar{H}^2 \right) \right],$$

... (4.9)

$$\bar{w} = -\frac{w_z}{\gamma} \left[ \frac{\partial}{\partial z} \left( P - \frac{1}{2} \sim_0 \bar{H}^2 \right) \right],$$

... (4.10)

where  $w_z$  is the permeability of the fluid in the porous region in axial direction, and  $P$  is the pressure there.

The continuity equation for the FF flow in the porous region is given by

$$\frac{1}{r} \frac{\partial}{\partial r} (r \bar{u}) + \frac{\partial \bar{w}}{\partial z} = 0.$$

... (4.11)

Substituting equations (4.9) and (4.10) in equation (4.11), and integrating over the thickness of the porous matrix  $H_0$ ; that is, over the interval  $(-H_0, 0)$  yields

$$\frac{1}{r} w_r H_0 \frac{\partial}{\partial r} \left[ r \frac{\partial}{\partial r} \left( P - \frac{1}{2} \bar{\omega}_0 \bar{H}^2 \right) \right] = -w_z \frac{\partial}{\partial z} \left( P - \frac{1}{2} \bar{\omega}_0 \bar{H}^2 \right) \Big|_{z=0} .$$

... (4.12)

Using Morgan-Cameron approximation [17] that the pressure  $P$  in the porous region can be replaced by the average pressure  $p$  with respect to the bearing wall thickness as

$$\frac{\partial}{\partial r} \left( P - \frac{1}{2} \bar{\omega}_0 \bar{H}^2 \right) = \frac{\partial}{\partial r} \left( p - \frac{1}{2} \bar{\omega}_0 \bar{H}^2 \right),$$

equation (4.12) becomes

$$\frac{\partial}{\partial z} \left( P - \frac{1}{2} \bar{\omega}_0 \bar{H}^2 \right) \Big|_{z=0} = -\frac{w_r H_0}{r w_z} \frac{\partial}{\partial r} \left[ r \frac{\partial}{\partial r} \left( p - \frac{1}{2} \bar{\omega}_0 \bar{H}^2 \right) \right].$$

... (4.13)

Assuming that the normal (axial) component of velocity across the film-porous interface at the lower plate are equal, therefore

$$w \Big|_{z=0} = \bar{w} \Big|_{z=0} .$$

... (4.14)

Using equations (4.8), (4.10), (4.13) and (4.14), one yields

$$\frac{1}{r} \frac{\partial}{\partial r} \left[ \left\{ 12\bar{w}_r \bar{H}_0 + \frac{h^3(4+sh)}{(1+sh)} \right\} r \frac{\partial}{\partial r} \left( \bar{p} - \frac{1}{2} \bar{\omega}_0 \bar{H}^2 \right) \right] = 12\gamma \dot{h}_m, \quad \dots (4.15)$$

which is known as Reynolds type equation of the considered phenomenon.

Introducing dimensionless quantities

$$R = \frac{r}{a}, \quad \bar{h}_m = \frac{h_m}{a}, \quad \bar{h} = \left( \frac{ah}{h_m^2} \right) \bar{h}_m, \quad \bar{H}_0 = \frac{H_0}{a}, \quad \bar{w}_r = \frac{w_r a}{h_m^3}, \quad \bar{\mathbb{E}}_r = \bar{w}_r \bar{H}_0, \\ \bar{s} = s h_m, \quad \bar{\omega}_0^* = -\frac{K \bar{\omega}_0 \bar{h}_m^3}{\gamma \dot{h}_m}, \quad \bar{p} = -\frac{h_m^3 p}{\gamma a^2 \dot{h}_m}. \quad \dots (4.16)$$

Equation (4.15) becomes

$$\frac{d}{dR} \left[ GR \frac{d}{dR} \left\{ \bar{p} - \frac{1}{2} \bar{\omega}_0^* R^2 (1-R) \right\} \right] = -12R, \quad \dots (4.17)$$

where

$$G = 12\bar{\mathbb{E}}_r + \frac{(\bar{h})^3(4+\bar{s}\bar{h})}{(1+\bar{s}\bar{h})}. \quad \dots (4.18)$$

### 4.3 Solution

Solving equation (4.17) under the boundary conditions for the pressure field as

$$\bar{p} = 0 \text{ when } R = 1 \quad \text{and} \quad \frac{d\bar{p}}{dR} = 0 \text{ when } R = 0,$$

... (4.19)

yields

$$\bar{p} = \frac{1}{2} \tilde{*} R^2 (1 - R) + \int_R^1 \frac{6R}{G} dR .$$

... (4.20)

The load carrying capacity  $W$  can be obtained by using the definition

$$W = 2f \int_0^a pr \, dr .$$

... (4.21)

Using dimensionless quantities defined in equation (4.16), equation (4.21) implies dimensionless load carrying capacity as

$$\bar{W} = -\frac{W h_m^3}{2f y a^4 h_m} = \frac{\tilde{*}}{40} + 3 \int_0^1 \frac{R^3}{G} dR ,$$

... (4.22)

where  $G$  is defined in equation (4.18).

Again, introducing dimensionless quantities for calculating response time  $t$  as

$$\bar{h}_i = \frac{h_m}{h_i}, \quad \tilde{\gamma}_1^* = \frac{K \tilde{\gamma}_0 \bar{a}^4}{W}, \quad W_r^* = \frac{W_r a}{h_i^3}, \quad \mathbb{E}_r^* = W_r^* \bar{H}_0, \quad \bar{t} = \frac{h_i^2 W t}{\gamma a^4}, \quad s^* = s h_i, \quad \dots (4.23)$$

where  $h_i$  is the initial film thickness.

Using (4.23), the dimensionless response time  $\bar{t}$  to reach a film thickness  $h_m$  starting with an initial film thickness  $h_i$  is given by

$$\frac{d\bar{t}}{d\bar{h}_i} = \frac{h_i^3 W}{\gamma a^4 h_m} = \frac{\int_0^1 \frac{3R^3}{G^*} dR}{\left( -\frac{1}{2f} + \frac{\tilde{\gamma}_1^*}{40} \right)}, \quad \dots (4.24)$$

which implies

$$\bar{t} = - \int_{\bar{h}_i}^1 \frac{\int_0^1 \frac{3R^3}{G^*} dR}{\left( -\frac{1}{2f} + \frac{\tilde{\gamma}_1^*}{40} \right)} d\bar{h}_i, \quad \dots (4.25)$$

where

$$G = \frac{G^*}{(\bar{h}_i)^3} \text{ and } G^* = 12\mathbb{E}_r^* + \frac{(\bar{h}_i)^3 \bar{h} (4 + s^* \bar{h}_i \bar{h})}{(1 + s^* \bar{h}_i \bar{h})}.$$

... (4.26)

## 4.4 Results and Discussion

The values of the dimensionless pressure distribution ( $\bar{p}$ ), load carrying capacity ( $\bar{W}$ ) and response time ( $\bar{t}$ ) have been calculated for the representative values of different parameters given in section 4.4.4 using Simpson's 1/3-rule with step size 0.1.

The FF used here is water based. The variable magnetic field considered is oblique to the lower plate and its strength is of  $O(10^2)$  in order to get maximum magnetic field strength at  $r = 2a/3$ . The calculation of magnetic field strength is shown in section 4.4.4. The other order of magnetic field strength with different  $K$  is shown in Figure 4.2.

When FF is used as lubricant, then the variation in  $\bar{p}$  is due to the first term of the equation (4.20). The same conclusion happens for  $\bar{W}$  in equation (4.22). Also, it is clear from equation (4.24) that, the variation in  $\bar{t}$  is due to the term  $\sim_1^*/40$ , when FF is used as lubricant.

### 4.4.1 Discussion on Squeeze Film Pressure

Figure 4.3 shows the variation in dimensionless pressure distribution  $\bar{p}$  as a function of dimensionless radial coordinate  $R$  for different values of dimensionless minimum film thickness  $\bar{h}_m$ . It is observed that  $\bar{p}$  increases as  $\bar{h}_m$  increases, but the increase rate is more when  $0 < R \leq 0.5$ . When  $R > 0.5$ , then  $\bar{p}$  remains almost same for all  $\bar{h}_m$ . That is, in general, as  $R$  increases,  $\bar{p}$  decreases. Hence,  $\bar{p}$  is maximum nearer to origin of radial axis. The variation

in  $\bar{p}$  as a function of dimensionless radial permeability parameter of the porous region  $\bar{w}_r$  is shown in Figure 4.4. It is observed that when  $2.92 \times 10^{-6} \leq \bar{w}_r \leq 2.92 \times 10^{-3}$ ,  $\bar{p}$  is constant, and then it starts decreasing when  $\bar{w}_r > 2.92 \times 10^{-3}$ . Figure 4.5 shows the variation in  $\bar{p}$  as a function of dimensionless thickness of the porous matrix  $\bar{H}_0$ . It is observed that for  $0 \leq \bar{H}_0 < 0.01$ ,  $\bar{p}$  remains constant. When  $\bar{H}_0 \geq 0.01$ ,  $\bar{p}$  starts decreasing. It should be noted here that  $\bar{H}_0 = 0$  indicates solid case; that is, the bearing design system without porous surface at bottom.

It is a general observation (refer [16, 18]) that, the insertion of porous surface decreases load carrying capacity and ultimately pressure. Moreover, porous surface is inserted because of advantageous property of self-lubrication. Thus, it is interesting to note from Figure 4.5 that when  $0 \leq \bar{H}_0 < 0.01$ ,  $\bar{p}$  remains constant. It means that,  $\bar{p}$  attains the same value as that of solid case ( $\bar{H}_0 = 0$ ) even if  $0 < \bar{H}_0 < 0.01$ . This is the added advantage of obtaining  $\bar{p}$  as that of solid case as well as maintaining self-lubricating property of bearing design system. From Figures 4.4 and 4.5,  $\bar{p}$  attains its maximum value, when  $2.92 \times 10^{-6} \leq \bar{w}_r \leq 2.92 \times 10^{-3}$  and  $0 < \bar{H}_0 < 0.01$ .

#### 4.4.2 Discussion on Load Carrying Capacity

Figure 4.6 shows the variation in dimensionless load carrying capacity  $\bar{W}$  as a function of dimensionless thickness of the porous matrix  $\bar{H}_0$  for different values of dimensionless minimum film thickness  $\bar{h}_m$ . It is observed that  $\bar{W}$  increases as  $\bar{h}_m$  increases. When  $0.005 \leq \bar{h}_m \leq 0.009$  and  $0.00001 \leq \bar{H}_0 \leq 0.01$ ,  $\bar{W}$  attains almost constant value. For  $0.001 \leq \bar{h}_m \leq 0.004$ ,  $\bar{W}$  starts decreasing after  $\bar{H}_0 = 0.0001$  whereas before that it takes constant value. After  $\bar{h}_m = 0.01$ ,  $\bar{W}$  decreases for all  $\bar{h}_m$ . The variation in  $\bar{W}$  as a function of

dimensionless radial permeability parameter of the porous region  $\bar{w}_r$  for  $\bar{h}_m = 0.007$  is shown in Figure 4.7. It is observed that  $\bar{w}_r$  has no effect on  $\bar{W}$ , when  $2.92 \times 10^{-6} \leq \bar{w}_r \leq 2.92 \times 10^{-3}$ . After  $\bar{w}_r > 2.92 \times 10^{-3}$ ,  $\bar{W}$  decreases. Thus, from Figures 4.6 and 4.7, it is observed that better load carrying capacity can be obtained for thin layer of FF, where  $0.005 \leq \bar{h}_m \leq 0.009$ ,  $0.00001 \leq \bar{H}_0 \leq 0.01$  and  $2.92 \times 10^{-6} \leq \bar{w}_r \leq 2.92 \times 10^{-3}$ . Figure 4.8 shows that  $\bar{W}$  attains the same value when  $\bar{H}_0 = 0$  (solid case) and  $\bar{H}_0 = 0.0001$ . Thus, again as discussed in squeeze film pressure, added advantage of obtaining  $\bar{W}$  as that of solid case with self-lubricating property of bearing design system is observed.

#### 4.4.3 Discussion on Squeeze Film Time

Solving equation (4.25) numerically using double integration procedure considering Simpson's 1/3-rule with step size 0.1 for inner integral and step size given by following calculation for outer integral.

$$\bar{h}_i = \frac{h_m}{h_i} = A \text{ (Say), then } \frac{1-A}{10} \Rightarrow \text{step size}$$

Figure 4.9 shows the variation in dimensionless response time  $\bar{t}$  as a function of dimensionless thickness of the porous matrix  $\bar{H}_0$  for different values of dimensionless minimum film thickness  $\bar{h}_m$ . It is observed that,  $\bar{t}$  decreases steeply when upper surface squeezing the FF film in the film region from height  $\bar{h}_i = 0.1$  to minimum film thickness  $\bar{h}_m = 0.001$ . When  $\bar{h}_m = 0.002$ , then decrease rate of  $\bar{t}$  becomes low. For all other values of  $\bar{h}_m$ ,  $\bar{t}$  almost takes constant value. It is to be noted here from Figure 4.9 that  $\bar{t}$  is more

when  $\bar{h}_m$  takes values from 0.009 to 0.001. The variation in  $\bar{t}$  as a function of dimensionless radial permeability parameter of porous region  $w_r^*$  for  $\bar{h}_m = 0.007$  is shown in Figure 4.10 where  $\bar{t}$  start decreases after  $w_r^* > 10^{-3}$ .

#### 4.4.4 Representative Values and Calculation of $K$

The following representative values are taken in computations.

$$h_i = 0.0001(m), \bar{z} = 0.05, y = 0.012 (Ns/m^2), y_r = 0.25, \sim_0 = 4f \times 10^{-7} (N/A^2),$$

$$K = 10^9 / 1.48 (A^2 / m^4), W = 25.0 (N), \dot{h}_m = 0.04 (m / s),$$

$$w_r = 10^{-11} (m^2) \text{ (fixed for Figures 4.3, 4.5, 4.6, 4.8, 4.9),}$$

$$H_0 = 0.0001(m) \text{ (fixed for Figures 4.3, 4.4, 4.7, 4.10),}$$

$$a = 0.001(m) \text{ (fixed for Figure 4.3), } a = 0.01 (m), \text{ (fixed for Figures 4.4 - 4.10),}$$

$$r = 0.0001(m) \text{ (fixed for Figures 4.4 - 4.10), } h_m = 0.00007(m) \text{ (fixed for Figures 4.4, 4.5).}$$

From equation (4.4),

$$H^2 = \frac{K r^2 (a - r)}{a},$$

$$\text{Max. } H^2 = 1.48 \times 10^{-5} K \text{ for } a = 0.01,$$

$$\text{For } K = 10^9 / 1.48, H = O(10^2) \text{ or } O(H) = 2,$$

where O indicates order.

## 4.5 Conclusions

On the basis of the ferrohydrodynamics theory, a FF lubricated squeeze film bearing design system formed by a sphere and a flat porous plate considering variable magnetic field, which is oblique to the lower plate, is theoretically analysed. It is noted here that porous plate is considered because of its advantageous property of self-lubrication and no need of exterior lubricant supply. The analytical model, known as Reynolds equation, is derived using equation of continuity in film as well as porous region and equations from ferrohydrodynamics theory. The above model also considers the validity of Darcy's law in the porous region.

The following conclusions can be made from results and discussion.

- (1)  $\bar{p}$  is maximum nearer to  $R = 0.1$
- (2)  $\bar{p}$  is maximum and constant, when  $2.92 \times 10^{-6} \leq \bar{w}_r \leq 2.92 \times 10^{-3}$
- (3)  $\bar{p}$  is maximum and constant, when  $0 < \bar{H}_0 < 0.01$
- (4) Better load carrying capacity can be obtained, when  $0.005 \leq \bar{h}_m \leq 0.009$ ,

$$0.00001 \leq \bar{H}_0 \leq 0.01 \quad \text{and} \quad 2.92 \times 10^{-6} \leq \bar{w}_r \leq 2.92 \times 10^{-3}$$

- (5)  $\bar{t}$  is maximum for  $\bar{h}_m = 0.001$ ,  $\bar{H}_0 = 0.00001$  and  $w_r^* = 10^{-6} - 10^{-3}$
- (6)  $\bar{t}$  has almost constant behaviour for  $0.003 \leq \bar{h}_m \leq 0.009$ .

It should be noted here that, according to [16], when porous layer is inserted then the pressure of the porous medium provides a path for the fluid to come out easily from the bearing to the environment, which varies with permeability. Thus, the presence of the porous material

decreases the resistance to flow in  $r$ -direction and as a consequence the load carrying capacity is reduced. The same behaviour also agrees with the conclusion of the Prakash and Tiwari [18] theoretically and experimentally by Wu [1]. In our case, the loss in  $\bar{W}$  due to effect of porosity is almost zero because of using FF as lubricant (which is controlled by oblique and variable magnetic field) for smaller values of  $\bar{H}_0$  and  $\bar{w}_r$ . Moreover, because of porosity effect, self-lubrication property is an added advantage. The present case reduces to the case of conventional lubricant when  $\bar{\omega}^* = 0$  and  $\bar{\omega}_1^* = 0$ .

It is to be noted here that variable magnetic field is used because uniform magnetic field does not enhance bearing performances as can be seen from equation (4.5).



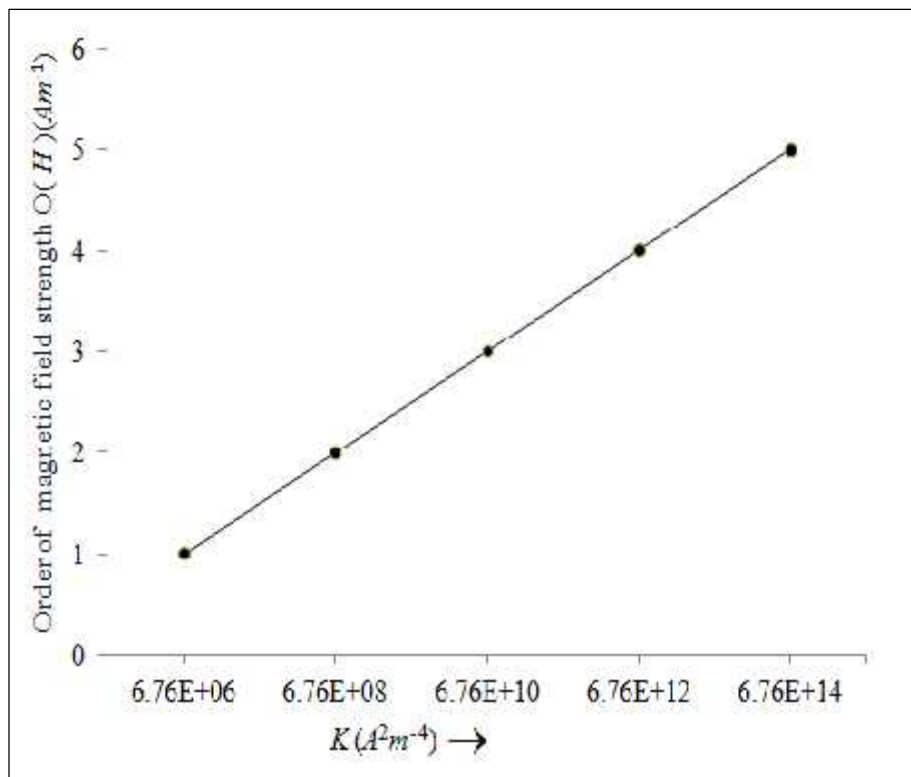


Figure 4.2 Order of magnetic field strength with different values of  $K$ .

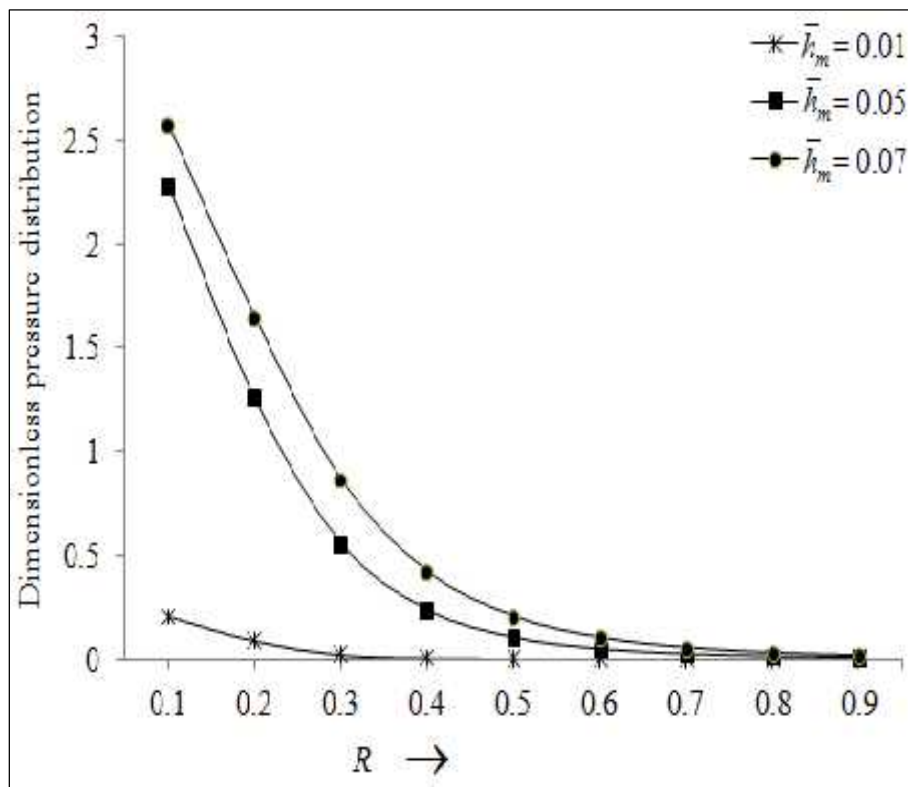


Figure 4.3 Variation in dimensionless pressure distribution  $\bar{p}$  for different values of  $R$  and  $\bar{h}_m$ .

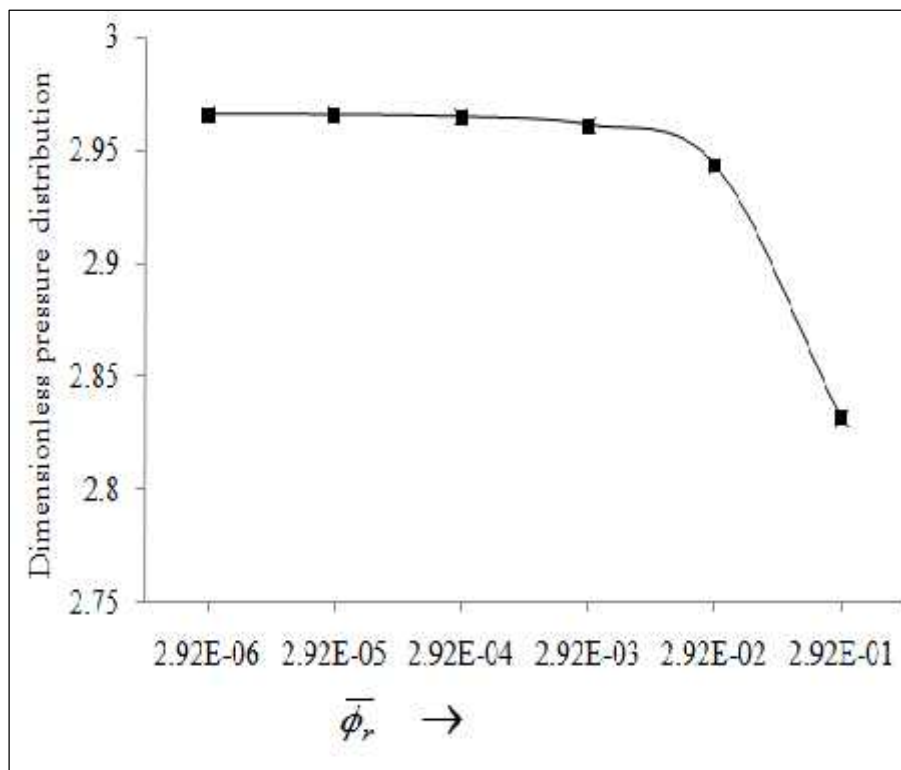


Figure 4.4 Variation in dimensionless pressure distribution  $\bar{p}$  for different values of  $\bar{\omega}_r$ .

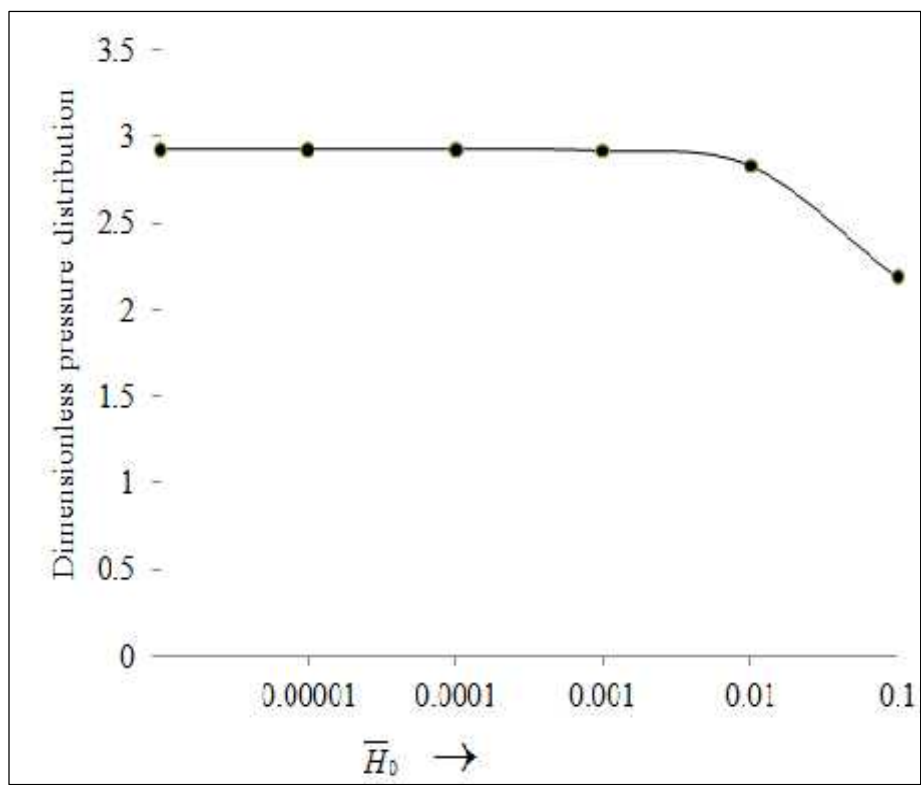


Figure 4.5 Variation in dimensionless pressure distribution  $\bar{p}$  for different values of  $\bar{H}_0$ .

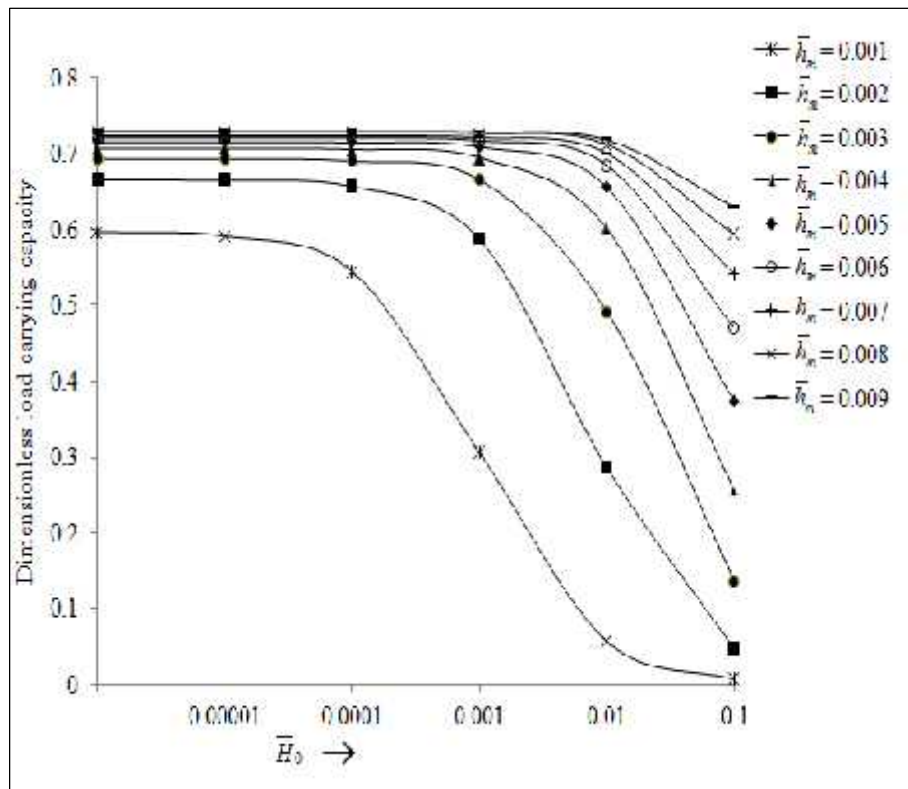


Figure 4.6 Variation in dimensionless load carrying capacity  $\bar{W}$  for different values of

$\bar{H}_0$  and  $\bar{h}_m$ .

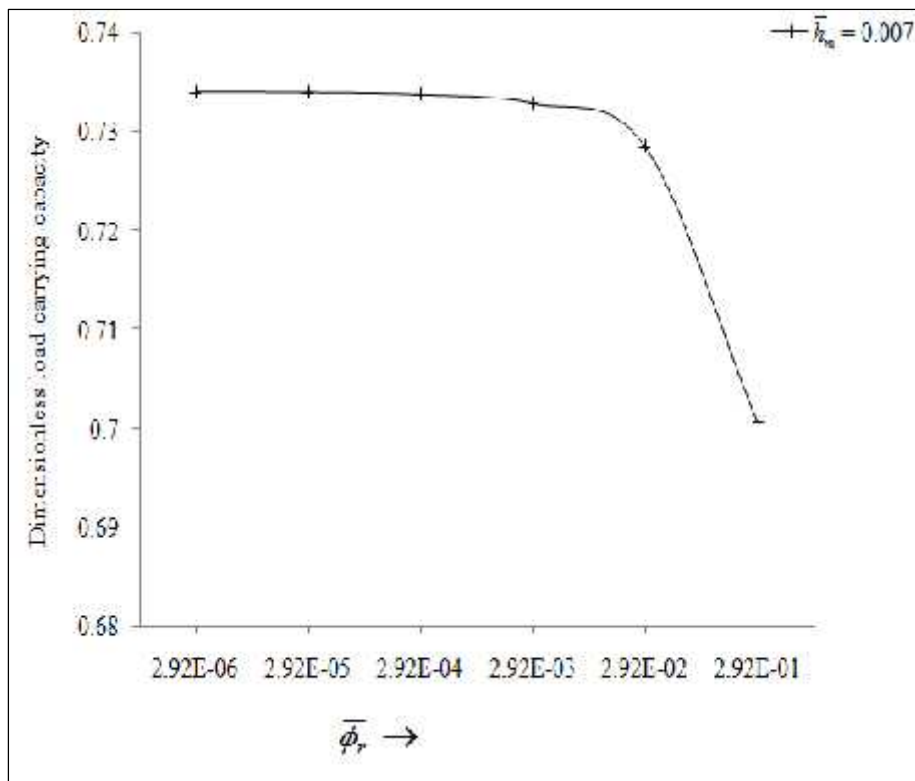


Figure 4.7 Variation in dimensionless load carrying capacity  $\bar{W}$  for different values of  $\bar{\phi}_r$ .

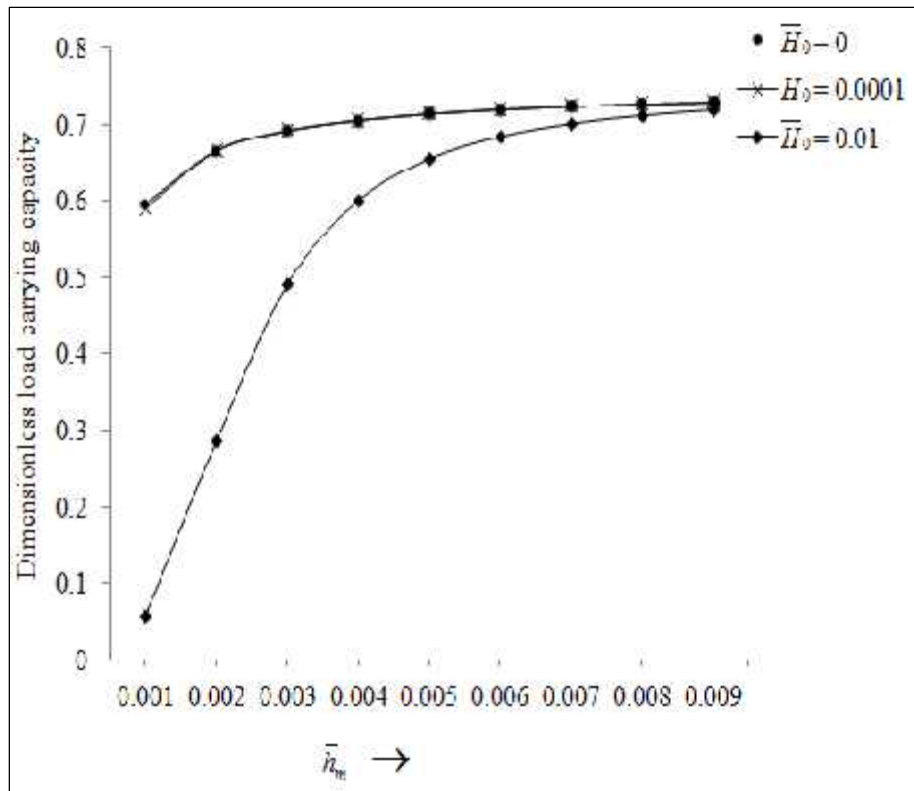


Figure 4.8 Variation in dimensionless load carrying capacity  $\bar{W}$  for different values of

$\bar{h}_m$  and  $\bar{H}_0$ .

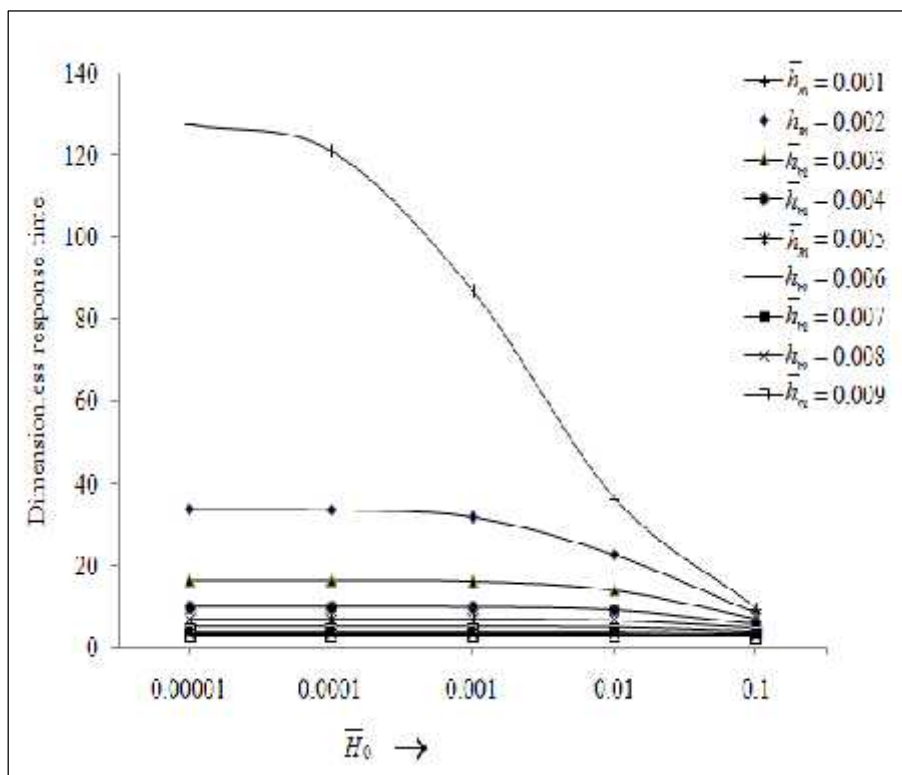


Figure 4.9 Variation in dimensionless response time  $\bar{t}$  for different values of  $\bar{H}_0$  and  $\bar{h}_m$  when squeezing takes place from height  $\bar{h}_i = 0.1$ .

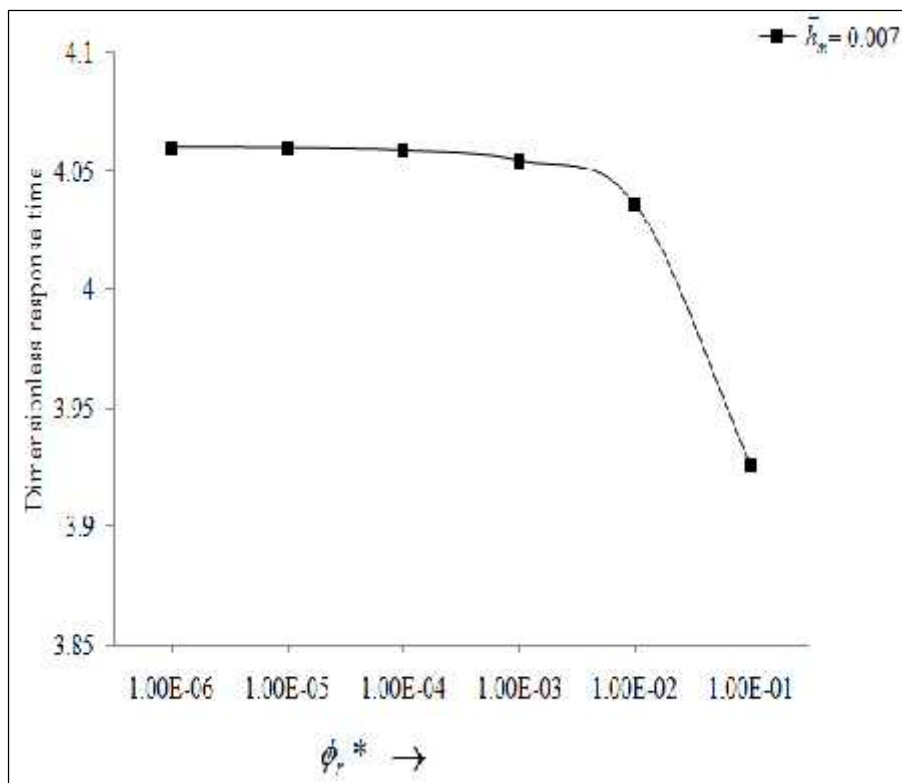


Figure 4.10 Variation in dimensionless response time  $\bar{t}$  for different values of  $w_r^*$  when squeezing takes place from height  $\bar{h}_i = 0.1$ .

## 4.7 References

- [1] Wu H, A review of porous squeeze films, *Wear*, 47, 371-385 (1978).
- [2] Naduvinamani N B and Katti S G, Micropolar fluid poro-elastic squeeze film lubrication between a cylinder and a rough flat plate – A special reference to synovial joint lubrication, *Tribology Online*, 9(1), 21-30 (2014).
- [3] Verma P D S, Magnetic fluid based squeeze film, *International Journal of Engineering Science*, 24(3), 395-401 (1986).
- [4] Kumar D, Sinha P and Chandra P, Ferrofluid squeeze film for spherical and conical bearings, *International Journal of Engineering Science*, 30(5), 645-656 (1992).
- [5] Bhat M V and Deheri G M, Magnetic-fluid-based squeeze film in curved porous circular discs, *Journal of Magnetism and Magnetic Materials*, 127, 159-162 (1993).
- [6] Prajapati B L, Magnetic-fluid-based porous squeeze films, *Journal of Magnetism and Magnetic Materials*, 149, 97-100 (1995).
- [7] Shah R C, Tripathi S R and Bhat M V, Magnetic fluid based squeeze film between porous annular curved plates with the effect of rotational inertia, *Pramana-Journal of Physics*, 58(3), 545-550 (2002).
- [8] Shah R C and Bhat M V, Ferrofluid squeeze film in a long journal bearing, *Tribology International*, 37, 441- 446 (2004).

- [9] Patel R M and Deheri G M, Magnetic fluid based squeeze film between porous conical plates, *Industrial Lubrication and Tribology*, 59(3), 143-147 (2007).
- [10] Andharia P I and Deheri G M, Effect of longitudinal roughness on magnetic fluid based squeeze film between truncated conical plates, *FDMP*, 7(1), 111-124 (2011).
- [11] Shah R C and Patel D B, Squeeze film based on ferrofluid in curved porous circular plates with various porous structures, *Applied Mathematics*, 2(4), 121-123 (2012).
- [12] Lin J R, Lin M C, Hung T C and Wang P Y, Effects of fluid inertia forces on the squeeze film characteristics of conical plates-ferromagnetic fluid model, *Lubrication Science*, 25, 429 - 439 (2013).
- [13] Lin J R, Lu R F, Lin M C and Wang P Y, Squeeze film characteristics of parallel circular disks lubricated by ferrofluids with non-Newtonian couple stresses, *Tribology International*, 61, 56-61(2013).
- [14] Shah R C and Bhat M V, Squeeze film based on magnetic fluid in curved porous rotating circular plates, *Journal of Magnetism and Magnetic Materials*, 208, 115-119 (2000).
- [15] Shah R C and Bhat M V, Anisotropic permeable porous facing and slip velocity on squeeze film in an axially undefined journal bearing with ferrofluid lubricant, *Journal of Magnetism and Magnetic Materials*, 279, 224-230 (2004).
- [16] Sparrow E M, Beavers G S and Hwang I T, Effect of velocity slip on porous-walled squeeze films, *Journal of Lubrication Technology*, 94, 260-265 (1972).

- [17] Shah R C and Bhat M V, Effect of slip velocity in a porous secant-shaped slider bearing with a ferrofluid lubricant, *FIZIKA A-ZAGREB*, 12(1), 1-8 (2003).
- [18] Prakash J and Tiwari K, Lubrication of a porous bearing with surface corrugations, *Journal of Lubrication Technology*, 104, 127-134 (1982).